Chemical Engineering Research and Design 203 (2024) 357–367

Contents lists available at ScienceDirect

Chemical Engineering Research and Design

journal homepage: www.elsevier.com/locate/cherd

Improving the analysis of heat transfer in packed beds: A comparative study between DEM simulations and existing literature models

C.L. Alves *, S. Heinrich

Institute of Solids Process Engineering and Particle Technology, Hamburg University of Technology (TUHH), 21073 Hamburg, Germany

ARTICLE INFO

Keywords:
Heat transfer
DEM modelling
Particle bed systems

ABSTRACT

The heat transfer within particle beds is of significant importance in various industrial applications; however, its comprehension remains limited. The investigation of packed beds involves employing the use of effective thermal conductivity, a widely employed approach that is constrained by the need for extensive experimental work and the presence of heterogeneities. Discrete Element Method (DEM) simulations are widely recognized as a valuable tool for enhancing comprehension of complex systems. Nevertheless, the extensive computational time required for these simulations poses a significant limitation on their widespread implementation. The present study encompassed the integration of particle-particle and particle-wall heat transfer models into the MUSEN framework. The models were employed to simulate scenarios involving stationary packed particle beds. The proposed models were validated by data obtained from existing literature. A favorable agreement was achieved for all examined instances, with notable reductions in simulation times, comparable to those observed in simulations employing the continuum approach. The simulations were compared with established models in the literature, and the simulations exhibited higher accuracy in predicting experimental values. This highlights the potential of the proposed methodology to be utilized in heat transfer analysis while maintaining efficient simulation times, without the need for continuum approach simulations, and providing additional understanding of the underlying micro mechanisms.

1. Introduction

Discrete particles can be found everywhere in science and industry because so many systems use suspensions, powder, composites, bulk solids, fluidized beds, packed beds, soil, or any combination of these. The analysis, planning, and optimization of industrial processes, as well as the comprehension of natural phenomena, are significantly influenced by the physicochemical and transport properties of materials. This is due to the fact that these materials exhibit distinct behavior compared to conventional single-phase systems. Recent years have seen a large number of theoretical-experimental studies on coupled heat and mass transfer in a variety of engineering fields, including food engineering, chemical engineering, geothermal engineering, drying technology, and others. However, there is still room for improvement in our fundamental knowledge of particulate system transport. The study of heat conduction holds significant importance across various academic areas, as it provides a fundamental understanding of thermal conduction phenomena necessary for analyzing heat transport systems (Vargas and McCarthy, 2001).

The following mechanisms have been identified for describing heat transfer within particle beds: thermal conduction through the solid, thermal conduction through the contact area between two particles, thermal conduction from the interstitial fluid, heat transfer by fluid convection, radiant heat transfer between the surfaces of particles, and radiant heat transfer between nearby particles (Borkink and Westerterp, 1992; Froment et al., 1990). Numerous correlations and methods have been developed to address heat conduction in granular media based on these mechanisms (Cheng et al., 2020; Peng et al., 2020; Tsotsas, 2019; Tsotsas and Martin, 1987; Wu et al., 2021). However, no unique solution to this problem has been discovered.

Some of the most common methods for studying these systems are currently based on a continuous macroscopic description, which involves the use of effective properties. Several analytical and empirical models have been developed to calculate the effective thermal conductivity of packed beds with and without the presence of a stagnant fluid (Kaviany, 2012). When applied to heterogeneous systems, however, none of these correlations yields consistent values for the fitting parameters. The effective thermal conductivity can be experimentally assessed using various techniques validated in continuum media

* Corresponding author.
E-mail address: carine.lourenco.alves@tuhh.de (C.L. Alves).

https://doi.org/10.1016/j.cherd.2024.01.062
Received 19 September 2023; Received in revised form 16 January 2024; Accepted 30 January 2024
Available online 3 February 2024

Nomenclature

A	Contact area (m^2)
$\dot{Q}$	Heat flow (W)
C_p	Particle heat capacity (J/kg K)
f_{res}	Thermal conduction resistivity factor (-)
$f_{res.eff}$	Effective thermal conduction resistivity factor (-)
Gr	Grashof number (-)
H_c	Effective heat conductance (W/K)
H	Bed height (M)
h	Heat transfer coefficient (W/m^2K)
k	Particle thermal conductivity (W/mK)
k_e^c	Effective thermal conductivity (W/mK)
k_{eq}	Equivalent thermal conductivity in contact (W/mK)
m	Mass (kg)
Nu	Nusselt number (-)
Pr	Prandtl number (-)
R_{eq}	Equivalent particle radius (m)
Re_h	Reynolds number (-)
R_i	Richardson number (-)
R_p	Particle radius (m)
S	Heat exchange surface (m^2)
S_l	Scaling up parameter for mass-length-dependent heat transfer (-)
T	Temperature (℃)
u_d	Darcy velocity vector (m/s)

Greek letters

a_v	Coefficient of thermal expansion (1/K)
β	Empirical constant (-)
ϕ	Empirical constant (-)
ε	Surface emissivity
ε_g	Void ratio (-)
φ	Porosity (-)
γ	Empiral constant (-)
δ	Packed thickness (m)
δ_n	Normal overlap (m)
λ_f	Thermal conductivity (W/mK)
$\lambda_{\min}$	Minimum overlap factor (m)
$\lambda_{\max}$	Maximum overlap factor (m)
ν_f	Kinematic viscosity (kg/ms)

Subscripts

conv	convection
c	contact
eq	equivalent
env	environment
f	fluid
p	particle
rad	radiation
s	solid
w	wall

(Presley and Christensen, 1997), but technical limitations and labor intensity make it nearly impossible to obtain this property manually. Additionally, the discrete nature of granular media and nonlinearity of contact interactions call into question the applicability of classical homogenization methods to describe particle collective behavior. As a result, reliable predictive methods based on proper heat conduction evaluation are desired (Dai, 2019). For this purpose, simulations can be successfully applied.

Using a continuum approach, partial differential equations expressing Fourier's law for thermal transfer processes are solved using an analytical approach or numerical methods such as the finite element method (FEM) to describe thermal processes in various applications (Druma et al., 2004; Sarikaya et al., 2005). However, the FEM becomes computationally intensive when considering structures heterogeneities and discontinuous media are considered. In this matter, DEM is a powerful tool to model granular material and microscale mechanics (Alves et al., 2023; Atrian et al., 2021). In recent years, the utilization of high-computational power, along with advanced parallel-computation algorithms has facilitated the successful application of DEM-based models in various thermal/reacting industrial processes. These models have enabled detailed analysis of the chemo-physics involved, even in scenarios where a large number of particles are present.

The first proposed model for conductive heat transfer when two particles are in contact was proposed by Batchelor and Brien et al. (Batchelor and O'Brien, 1977) in the case of conductive heat transfer between two particles resulting from static contact. On the proposed model, the heat flux across the particle boundary between a particle 1 and 2 is defined according to:

$$Q_{12} = H_c(T_1 - T_2) \tag{1}$$

In which, H_c englobes the effective heat conductance in W/K.

The equation is valid for static contacts in cases where Eq. (2) is applicable:

$$k_s r_c / k_f r_p \gg 1 \tag{2}$$

In which, r_c represents the contact radius, $r_p$represents the radius of the rigid particle, $k_s$and $k_f$are used to represent the thermal conductivities of solid particles and the fluid, respectively.

In cases where the conduction between two particles is influenced by interstitial fluid, specifically when the proposed condition on Eq. (2) is not met, Rong&Horio (Rong and Horio, 1999) introduced a novel approach known as the surrounding layer method, which aims to establish the conditions and methodology for incorporating indirect conduction via the interstitial fluid. Tsory et al. (Tsory et al., 2013) introduced a simplified approach that involved partitioning particle contact into two components: solid-solid contact and air gaps. To determine conductive heat transfer, they simply added the conduction through these two components. The direct additional, nevertheless, fails to resolve every reported case. Additional complex solutions were proposed as the one by Cheng et al. (Cheng et al., 2020), Rodrigues et al. (Rodrigues et al., 2022) and Fischer et al. (Fischer et al., 2023).

The present study describes heat transfer models on DEM to investigate thermal conduction phenomena including both solid-to-particle and particle-to-particle interactions. This model aims to comprehensively address all possible scenarios limited by Eq. (2) and improve simple propose models without the requirement of further advanced approaches that lead to high computational costs and simulation times, but at the same time consider more the micro-scale level by modelling individual particle interactions, granular rearrangements, and complex contact physics, offering a more detailed and realistic representation of the system specially compared to continuum approach simulations as FEM.

The proposed models were implemented on MUSEN open source framework and validated based on different experimental data from the literature (Mishra et al., 2019; Vargas and McCarthy, 2001), highlighting the wide range of applicability of the proposed models. MUSEN was created to perform efficient calculations on personal computers equipped with general-purpose graphics (GPUs) processing units, allowing thermal conduction simulations to be completed in a short amount of time and efficiently determining the effective thermal

conductivity of particle beds.

2. Materials and methods

2.1. Numerical modelling in DEM

The implementation of the proposed heat transfer models was done on MUSEN framework (Dosta and Skorych, 2020). MUSEN is an open-source DEM simulation framework. MUSEN is based on the soft-sphere discrete element method. For time integration, the leap-frog algorithm is commonly employed as a numerical method. The implementation utilizes the Verlet (Verlet, 1967) list approach in conjunction with the linked-cell algorithm (Quentrec and Brot, 1973) for contact detection. The multigrid approach supports a faster processing of particle sets with wide size distributions.

Ultimately, the Verlet list is populated with interactions that have the potential to occur within a defined cut-off distance. This implies that it possesses the capability to be utilized without the need for recalibration throughout multiple sequential calculation iterations. Consequently, the choice of the most suitable threshold distance can have a substantial impact on the accuracy and effectiveness of computations. One potential drawback is that bigger numbers result in increased memory usage and larger lists of potential contacts, necessitating analysis in each time step. In contrast, shorter distances necessitate more frequent iterations of list recalculations. Hence, a methodology for the automated adaptation of the threshold distance has been devised and included into the MUSEN system. The primary performance metric analyzed is the average execution time of a single DEM simulation phase. The recalculation of the cut-off distance occurs after a predetermined number of steps, considering the performance data obtained from the previous cut-off distances. This enables the consideration of the present computational resource load, encompassing both CPU and GPU, in order to determine an ideal value based on the prevailing conditions.

The calculations on the GPU are executed utilizing the CUDA computing platform, enabling the simulation of scenes comprising several discrete objects within a feasible timeframe (Dosta et al., 2020). In the context of GPU computing, a hybrid methodology is employed, wherein the CPU is responsible for touch detection, while the GPU handles the computation of forces and the integration of motion. The Verlet list, computed on CPU, comprises both presently active contacts and a collection of all possible contacts that may arise during a designated time interval defined by the cut-off distance. Therefore, the necessity to transport data between the CPU and GPU after each step is eliminated, resulting in a substantial enhancement in computational efficiency. However, this approach also leads to an augmented demand for memory resources on the GPU. During each iteration, the GPU evaluates the precise coordinates of the particles from the given list of potential contacts, resulting in the generation of a reduced list of active contacts.

The following assumptions were made in the developed model:

1. The main heat transfer mechanism is through conduction between solid particles;
2. The fluid surrounding the particles remains stagnant;
3. The conductivity of the interstitial fluid is relatively small compared to that of the particle;
4. Temperatures remain continuous across all interfaces;
5. The adsorption of gas on the surface of particles is negligible
6. All phases are inert and thermally stable.

The heat flow between colliding particle and wall was modelled based on Jarolin et al. (Jarolin et al., 2022):

$$\dot{Q}_{part-wall} = hAf_{res}(T_w - T_p) \tag{3}$$

where h is the heat transfer coefficient in W/m^{2}K, A is the contact area in m^2, f_{res} is the thermal conduction resistivity factor, wall temperature and T_p is the particle temperature.

The contact area A is calculated as:

$$A = \pi {R_c}^2 = \pi R_p \delta_n \tag{4}$$

where R_c is the contact radius of the particle with the wall, $R_p$is the particle radius and δ_n is the normal overlap between wall and particles. Between colliding particles, heat flow due to conduction was modelled based on (Teixeira et al., 2021):

$$\dot{Q}_{part-part} = 2R_c S_l f_{res,eff} k_{eq}(T_1 - T_2) \tag{5}$$

here R_c is the contact radius between particles in m, S_l is the scaling parameter for mass-length-dependent heat transfer, $f_{res,eff}$ is an effective thermal conduction resistivity factor, k_{eq} is the equivalent thermal conductivity in contact in W/mK and T_1 and T_2 particles temperature.

The contact radius R_c was derived from Coble geometric model based on the radii R_1 and R_2 from the particles as (Besler et al., 2015):

$$R_c = 2\sqrt{R_{eq}\delta_n}, \tag{6}$$

$$R_{eq} = \frac{R_1 R_2}{R_1 + R_2} \tag{7}$$

in which, δ_n is the normal overlap between particles in m. The normal overlap is calculated based on the particle positions and their radii as formulated by Hertz-Mindlin model.

Similarly to the equivalent particle radius R_{eq} determined by Eq. (7), the equivalent thermal conductivity is according to Eq. (8):

$$k_{eq} = \frac{k_1 k_2}{k_1 + k_2} \tag{8}$$

where k_1 and k_2 are the thermal conductivity of particle 1 and 2, respectively. The effective thermal conduction resistivity factor $f_{res,eff}$ varies according with the normal overlap:

$$f_{res,eff} = \begin{cases} f_{res} \quad , \delta_n \le 2\lambda_{\min} R_{eq} \\ f_{res} + \dfrac{1 - f_{res}}{\lambda_{\max} - \lambda_{\min}} \left(\dfrac{\delta_n}{2R_{eq}} - \lambda_{\min} \right), 2\lambda_{\min} R_{eq} \le \delta_n \le 2\lambda_{\max} R_{eq} \\ 1, 2\lambda_{\max} R_{eq} \le \delta_n \end{cases} \tag{9}$$

where, f_{res} is thermal conduction resistivity factor, $\lambda_{\min}$ is a minimum overlap factor and $\lambda_{\max}$ is a maximum overlap factor.

The proposed modifications depend on the $f_{res,eff}$ factor, which accounts for the different overlap in the particles contact and the scaling parameter for mass-length-dependent heat transfer S_l that will account for the heat transfer between particles i and j($\dot{Q}_{part-part}$) and the indirect

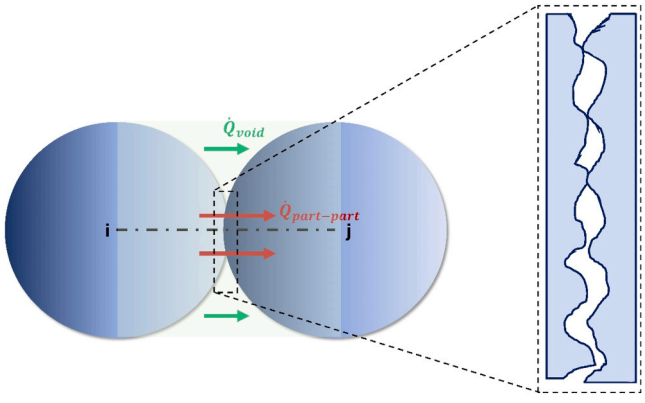

Fig. 1. Schematic description of the proposed heat transfer model between particles.

conduction heat transfer via voids ($\dot{Q}_{void}$) as schematic shown in Fig. 1:

Heat flow between the particle and the environment are due to convection and radiation and were modelled according to Eq. (10) to (12), respectively:

$$\dot{Q}_{ext} = \dot{Q}_{ext,conv} + \dot{Q}_{ext,rad} \tag{10}$$

$$\dot{Q}_{ext,conv} = khS(T_{env} - T_p) \tag{11}$$

$$\dot{Q}_{ext,rad} = k\varepsilon S({T_{env}}^4 - {T_p}^4) \tag{12}$$

where h is the heat transfer coefficient in W/m^{2}K, S is the heat exchange surface m^2, k is the scaling factor,ε is the surface emissivity, T_{env} is the environment temperature and T_p is the particle temperature. The heat transfer coefficient h is modelled according to the type of convection in the system.

The integration of heat in a particle i is done according to:

$$\dot{Q}_i = \sum \vec{\dot{Q}}_{part-part} + \vec{\dot{Q}}_{part-wall} + \vec{\dot{Q}}_{env} \tag{13}$$

$$T_i = T_i + \frac{\dot{Q}_i}{C_{p,i} m_i} \Delta t_{sim} \tag{14}$$

where the C_i is the heat capacity of particle i [J/kg K] and m_i is the particle mass. The total heat flux is given by the contributions of the heat flux between each particle contact and particle-wall. The temperature is integrated in each time step according to the simulation time step Δt_{sim}.

In order to produce a uniform arrangement of particles, a force-biased algorithm was implemented to generate the particle packaging (Dosta et al., 2019). Particles are initially generated at random within the specified volume by this algorithm. Following the detection of particle contacts, the calculation of virtual forces in the normal directions ensues. These forces are utilized to reduce the overlap of the particles until the utmost overlap specified is achieved. Following the generating process, the particles are arranged to fall in accordance with the experimental specifications as described in the sequence, so creating the particle beds. To investigate the impact of the random production and falling of particles, the process of generating particles in the volume and forming the particle bed was repeated five times in order to observe its effect on the simulation results.

The simulation results were validated based on the R-squared values between the simulated values and experimental data on a point-by-point basis. The simulated temperature values on the packed material have been assessed using the same methodology as described in the experimental data (seen in the next section), in order to allow for an accurate comparison. To ensure the identification of the minimum R^2 value, the simulation was iterated ten times to validate the obtained results.

2.2. Experimental data

The proposed models were validated based on the experimental data developed by Vargas et al. (Vargas and McCarthy, 2001) and Mishra et al. (Mishra et al., 2019). The two approaches align with the methodologies described in the available literature on the issue (Dai, 2019; Deissler and Boegli, 1958; Jayachandran and Reddy, 2019; Kunii and Smith, 1960; Nield, 1991; Qian et al., 2018).

Vargas et al. (Vargas and McCarthy, 2001) carried out experiments using a heated Hele-Shaw like device, which allows a mono-layer of cylindrical particles to be uni-axially loaded. Two walls (as well as the front and back plates) are insulated, while the other two are heated and/or cooled. The temperature profiles within the bed were obtained using liquid crystal thermography. The system allows the investigation of heat transfer in a quasi-static configuration. The top view of the apparatus can be seen in Fig. 2:

The bottom wall was kept at 50 ℃, while the remaining walls were insulated on the basis of a vacuum system. The initial temperature of the particles was 25 ℃ and a one-dimensional loading is imposed on the upper wall and the effective thermal conductivity for loads of 5, 10, 15 and 20 kgf is compared between the simulation and experiments for 155-min heating. The effective thermal conductivity for 2D rectangular beds is given by equation according to Eq. (15) (Slavin et al., 2000b):

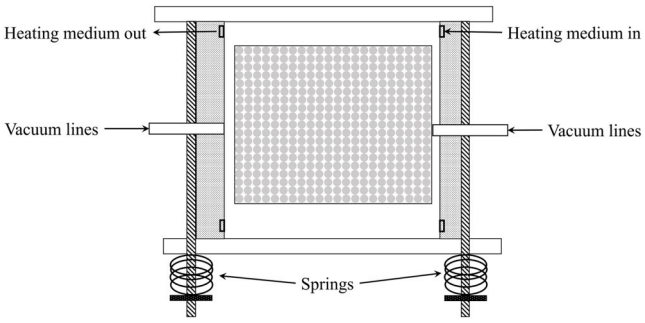

Fig. 2. Top view of the experiment setup developed by Vargas et al. (Vargas and McCarthy, 2001).

$$k_{eff} = -\frac{Q}{\left(\frac{Wd_p}{H}\right)\Delta T} \tag{15}$$

in which, H is the bed height, W is the bed width, d_p is the particle diameter, ΔT the temperature gradient within the bed height and Q is the heat flow through the bottom wall.

Considering the vacuum isolation systems, the heat transfer coefficient h (s. Eq. (11)) was assumed to be zero. The radiation was also disregarded because of the temperature regimes. The system was composed of dispersed stainless-steel SS-304 spheres forming a 3D packed bed (0.3 ×30.4 ×45 cm^3). Table 1 describes the applied simulation parameters:

The simulation time step was $7 \bullet 10^{-5}$ s compared to $1 \bullet 10^{-7}$ reported by Vargas et al. (Vargas and McCarthy, 2001). This value was determined based on a convergence test as 1/2000 of Rayleigh time. The simulations scene was of 15.5 s to replicate the 155 min of the experiment. The 155-minute experiment was used to validate the model parameters and the simulations were then compared to the experimental data of 60 and 10 min.

The experiments carried out by Mishra et al. (Mishra et al., 2019) aimed to evaluate the wall -particle heat transfer to determine the specific heat transfer (h) for the particles. The experimental setup was proposed according to Fig. 3:

The experimental setup consists of an aluminum block (5 cm × 5 cm x 8 cm) and an aluminum particle holder (5 cm × 5 cm x 5 cm). The heating system is a 20 W Watlow square heating element that maintains a constant temperature of 70 °C. The whole system is placed inside a Styrofoam box to minimize heat loss from the side walls. The temperatures are recorded by Micro-beta chip NTC thermistors. Particles at room temperature (assumed as 20 ℃) are dropped onto the top surface of the hot aluminum block. The temperature on the particle bed is measured and evaluated to obtain the bed temperature profile.

Table 1
Parameter applied on the simulations of static bed simulations proposed by Vargas et al. (Vargas and McCarthy, 2001).

Property	Value
Density [kg/m^3]	7500
Poisson ratio [-]	0.29
Young's Modulus [GPa]	193
Particle diameter [m]	$3 \bullet 10^{-3}$
Thermal conductivity [W/mK]	15
Heat capacity [J/kgK]	440
Number of particles [-]	15548

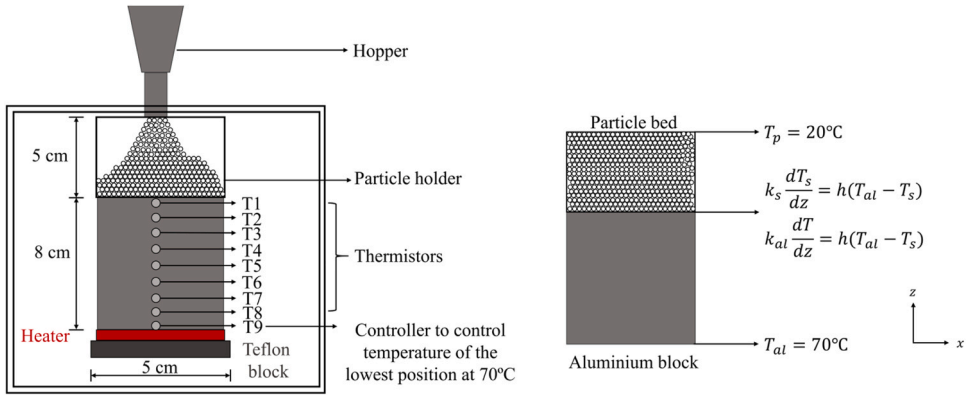

Fig. 3. Experimental setup proposed by Mishra et al. (Mishra et al., 2019) for the investigation of wall-particle heat transfer.

The experiments were carried out for glass and steel particles. And different average particle sizes of glass (165 μm, 275 μm and 462 μm). The particles were generated in a domain of 2 cm × 2 cm × 4 cm with porosity of 0.58 and let the particles fall to generate the particle bed on a 5 cm × 5 cm × 5 cm cube as the experiment. For the analysis of 165 μm, 275 μm and 462 μm glass particles as well as 1 mm steel particles, the simulation scenes total 2857056, 617124, 130150, and 12834 particles, respectively. The applied time steps were $9 \bullet 10^{-9}$ s, $1.5 \bullet 10^{-8}$ s,$2.5 \bullet 10^{-8}$ s and $5.2 \bullet 10^{-8}$ s for the simulations of 165 μm, 275 μm and 462 μm glass particles as well as 1 mm steel particles. These values were determined by a convergence test.

The natural convection intensity in the packed bed primarily relies on the Grashof number (*Gr*), using the spherical diameter (d_p) as the characteristic scale (Lee et al., 2017). The Grashof number is determined according to:

$$Gr = \frac{g a_v \Delta T d_p^3}{\upsilon_f^2} \tag{16}$$

in which, a_v is the coefficient of thermal expansion, υ_f is the kinematic viscosity of the heat transfer fluid and ΔT is the temperature difference between the particles and air. It should be noted that the *Gr* number is directly proportional to the temperature difference between particles and air. As the temperature of the particles decreases, the *Gr* number decreases as well, leading to a decrease in the intensity of natural convection.

Given an initial temperature difference of 50 °C between the particle bed and room temperature, and assuming the coefficient of thermal expansion of air at room temperature to be 0.0034/K and υ_f to be $1.825 \bullet 10^{-5}$ kg/ms (Bastian E. Rapp, 2017), *Gr* number is calculated to be 0.0369, 0.153, 0.81, and 8.22 for systems consisting of glass particles with diameters of 165 μm, 275 μm, and 462 μm, as well as 1 mm steel particles.

The distinction between the magnitudes of natural and forced convection in mixed convection is primarily indicated by the Richardson number (*Ri*). Typically, the impact of natural convection can be disregarded when $Ri < 0.1$ and the impact of forced convection can be disregarded when $Ri \geq 10$. The *Ri* number can be calculated according to:

$$Ri = \frac{Gr}{\mathrm{Re}_h^2} \tag{17}$$

here Re_h is the Reynolds number. The Reynolds number in turn for packed bed can be determined according to (Demirel et al., 2000):

$$\mathrm{Re}_h = \frac{(|u_d|/\varepsilon)}{\upsilon_f} \frac{4\varepsilon}{1-\varepsilon} \left(\frac{V_p}{A_p}\right) \tag{18}$$

in which, ε is the porosity of the bed, u_d is Darcy velocity vector, A_p is the surface area of the particle bed and V_p is the volume of the particle bed. Approximating the particles as perfect spheres, Eq. 18 can be simplified to:

$$\mathrm{Re}_h = \frac{(|u_d|/\varepsilon)}{\upsilon_f} \frac{4\varepsilon}{1-\varepsilon} \left(\frac{d_p}{6}\right) \tag{19}$$

Considering the system with basically stagnant air, u_d have been reported to vary from 10^{-6} to 10^{-3} m/s (Shruti et al., 2023). Therefore, the Re_h varied from $1.77 \bullet 10^{-5}$ to 0.0177 for the system containing glass particles with a size of 165 μm, from $2.84 \bullet 10^{-5}$ to 0.0284 for the system with 275 μm particles, from $4.95 \bullet 10^{-5}$ to 0.0495 for the system with 462 μm particles and $1.07 \bullet 10^{-4}$ to 0.107 for the system with 1 mm steel particles.

The *Ri* numbers for the systems can be determined as follows: for the system containing glass particles with a size of 165 μm, *Ri* number ranges from $1.18 \bullet 10^{8}$ to 118; for the system with 275 μm particles, *Ri* number ranges from $1.89 \bullet 10^{8}$ to 189; for the system with 462 μm particles, *Ri* number ranges from $3.30 \bullet 10^{8}$ to 330 and for the system with 1 mm steel particles, *Ri* number ranges $7.14 \bullet 10^{8}$ to 714. As a result, while the effects of forced convection can be ignored in all situations, it is necessary to consider the impact of natural convection.

The natural convection correlation for a single sphere proposed by Churchill (Churchill, 1983) is expressed as:

$$Nu_N = \frac{h_{sf} d_p}{\lambda_f} = 2 + \frac{0.589 Ra^{1/4}}{\left[1 + \left(\frac{0.469}{\mathrm{Pr}}\right)^{\frac{9}{16}}\right]^{4/9}} \tag{20}$$

in which, h_{sf} is the convective heat transfer coefficient, λ_f is the thermal conductivity of the heat transfer fluid, Pr is the Prandtl number and *Ra* is the measure of flow strength resulting from buoyancy, which can be determined using the following formula:

$$Ra = Gr \bullet \mathrm{Pr} \tag{21}$$

Prandtl number for air have been reported as 0.72 (Bastian E. Rapp, 2017). As a result, the *Ra* values for the different particle systems are as follows: $2.66 \bullet 10^{-2}$ for the system of 165 μm particles, $1.1 \bullet 10^{-1}$ for the system of 275 μm particles, $5.83 \bullet 10^{-1}$ for the system of 462 μm particles and 5.92 for 1 mm steel particles. Lee et al. (Lee et al., 2017) reported that the natural convective heat transfer coefficient in a packed bed is in good agreement Eq. (20) for a low Ra, similar to the calculated values.

Assuming the thermal conductivity of the heat transfer of air as $2.74 \bullet 10^{-2}$ W/mK (Bastian E. Rapp, 2017), the Nusselt number was determined as: 2.18 for the system of 165 μm particles, 2.26 for the system of 275 μm particles, 2.40 for the system of 462 μm particles and 2.71 for 1 mm steel particles. Consequently, the convective heat transfer coefficient could be determined as 362.88, 234.06, 142.3 and 74.3 W/

m^2K for the system with 165 μm, 265 μm, 462 μm and 1 mm particles. The values were utilized to model the heat loss to the environment based on Eq. (12).

The remaining applied parameters of the experiments and utilized on the simulations are seen in Table 2:

For all simulations, a time factor of $1•10^3$ was applied to minimize the simulation time. Consequently, the heat transfer parameters for all simulated models were adjusted to maintain physical accuracy and ensure that the simulation results remained consistent with the original heat transfer behavior. This allowed the simulation of 165 μm particles bed to be minimized from 112 days to approximately 57 min (using a NVIDIA GeForce RTX 2060 SUPER graphic card), compared to the 118 days reported by Mishra et al. (Mishra et al., 2019) (using 42 Intel(R) Xeon(R) 2.40 GHz processors in parallel).

The simulation model parameters for both the particle wall and particle particle models were adjusted according to the transient solution after 1 s of the particle bed of 165 μm obtained by Mishra et al. (Mishra et al., 2019) and the adjusted values were applied for the other simulations of the different particle sizes and the heat transfer coefficients from simulations and experiments were compared. To calculate the heat transfer coefficient predicted by DEM simulations, the wall-to-particle heat rate and particle temperature are averaged over time (t_{avg}). The heat transfer coefficient for the bottom plate (h_{DEM}) is calculated by dividing the total heat rate ($\dot{q}_{total}$) by the surface area of the bottom wall (A_{wall}= 25 cm^2) and the temperature difference between the wall and the particles, the calculation can be seen in Eq. (22):

$$h_{DEM} = \frac{\dot{q}_{total}}{A_{wall}(T_w - T_{p,avg})} \tag{22}$$

Assuming steady-state conduction, the heat transfer coefficient h and effective thermal conductivity k_{eff} can be corelated by the thickness of the bed δ according to:

$$h = \frac{k_{eff}}{\delta} \tag{23}$$

For the developed DEM simulation, the temperature wall was considered to be 68.5 °C, considering the thermistors reading for the aluminum block as seen in Fig. 4. The error bars are due the accuracy of thermistors of ± 0.2 °C:

The temperature analysis over bed height was performed by averaging the particles within 0.5 cm and 1 cm layers as exemplified in the 165 μm particle bed in Fig. 5:

The analysis of particle size with the resistivity factor could be developed after validation on the 165 μm particle bed and the heat transfer coefficient between the experiments and simulations was compared.

The methodology employed in both experimental situations was utilized to ascertain the temperature of the particles during the experiments. This served as the basis for establishing the temperature of the particles in the simulations, so ensuring consistency between the simulated and experimental results. Different models of effective thermal conductivity were utilized to compare and ascertain the effective

Table 2
Simulation parameters for the experimental developed by Mishra et al. (Mishra et al., 2019).

Property	Glass	Steel	Aluminium
Particle diameter [m]	$165•10^{-6}$, $275•10^{-6}$, $462•10^{-6}$	$1•10^{-3}$	
Density [kg/m^3]	2500	7810	2700
Poisson ratio [-]	0.17	0.28	0.33
Young's Modulus [GPa]	72	200	69
Thermal conductivity [W/mK]	1.1	46.6	167
Heat capacity [J/kgK]	795	502	896
Time factor [-]	$1•10^3$	$1•10^3$	$1•10^3$

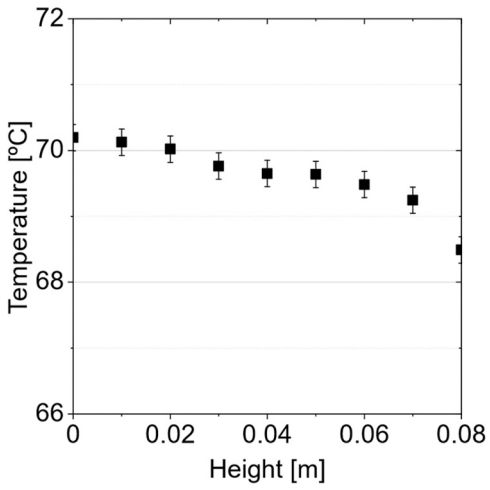

Fig. 4. Temperature readings of the aluminum block from Mishra et al. (Mishra et al., 2019).

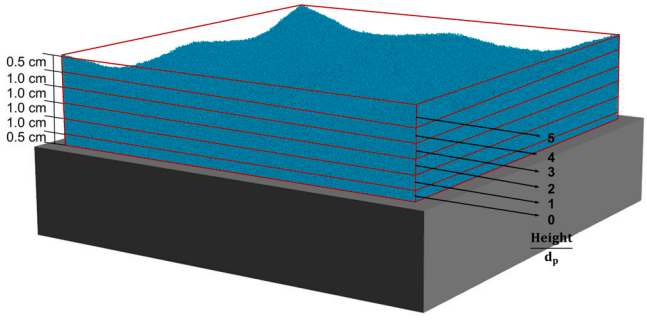

Fig. 5. Description of procedure for temperature analysis on particle bed exemplified on the 165 μm particle bed.

thermal conductivity of both experiments. Table 3 summarizes the applied correlations (Bauer, 1978; Deissler and Boegli, 1958; Jayachandran and Reddy, 2019; Nield, 1991; Qian et al., 2018; Yagi and Kunii, 1957; Zehner and Schlünder, 1970).

here k_e^c is the effective thermal conductivity of the bed due to thermal conduction on W/(mK), k_g is the effective thermal conductivity of the gas phase, W/(mK) and ε_g is the void ratio. Void ratio ε_g is defined as the volume of voids divided by the total volume of solid particles, whereas porosity φ is defined as the volume of voids divided by the total volume of the sample (solids and voids combined). Consequently, the void ratio

Table 3
Semi empirical models from the literature for effective thermal conductivity.

Model	Effective thermal conductivity	Reference
Parallel layers	$\frac{k_e^c}{k_g} = \varepsilon_g + (1-\varepsilon_g)K$	(Deissler and Boegli, 1958)
Series layers	$\frac{k_e^c}{k_g} = \frac{1}{\varepsilon_g + (1-\varepsilon_g)/K}$	(Deissler and Boegli, 1958)
Geometric mean	$\frac{k_e^c}{k_g} = K^{(1-\varepsilon_g)}$	(Nield, 1991)
Kunii and Smith (KS)	$\frac{k_e^c}{k_g} = \varepsilon_g + \frac{\beta(1-\varepsilon_g)}{\frac{1}{\phi} + \frac{d_p h_p}{k_g} + \gamma\left(\frac{k_g}{k_s}\right)}$	(Yagi and Kunii, 1957)
Zehner and Schlünder (ZS)	$\frac{k_e^c}{k_g} = (1-\sqrt{1-\varepsilon_g}) + \sqrt{1-\varepsilon_g}\Gamma$	(Zehner and Schlünder, 1970)
Zehner-Bauer-Schlünder (ZBS)	$\frac{k_e^c}{k_g} = (1-\sqrt{1-\varepsilon_g}) + \sqrt{1-\varepsilon_g}[\omega K + (1-\omega)\Gamma]$	(Bauer, 1978)

ε_g and porosity φ are correlated as

$$\varepsilon_g = \frac{\varphi}{1 - \varphi} \tag{24}$$

The void ratio ε_g of the bed of particles, also named intergranular porosity, was determined assuming completed solid particles for both proposed experiments.

K is a dimensionless parameter calculated by the ratio between the thermal conductivity of the solid (k_s) and the thermal conductivity of the gas phase (k_g). The thermal conductivity of gas was assumed to be 0.024 W/mK (Graczykowski et al., 2017).

β andγ are empirical parameters assumed as $\sqrt{3}/3$ and 0.666, respectively, according to both investigated packing (Deissler and Boegli, 1958). The empirical constant ϕ for KS model was calculated by (Yagi and Kunii, 1957):

$$\begin{aligned} &or \quad 0.26 \le \varepsilon_g \le 0.476 \quad \phi = \phi_2 + (\phi_1 + \phi_2)\frac{\varepsilon_g - 0.26}{0.216} \\ &for \quad \varepsilon_g \ge 0.476 \qquad\qquad \phi = \phi_1 \\ &for \quad \varepsilon_g \le 0.26 \qquad\qquad \phi = \phi_2 \end{aligned} \tag{25}$$

where ϕ_1 refers to lose packing arrangement ($\varepsilon_g \ge 0.476$) and ϕ_2 refers to tight packing arrangement ($\varepsilon_g \le 0.26$). ϕ_{1or2} can be calculated as:

$$\phi_{1or2} = \frac{0.5((K-1)/K)^2 1/n}{\ln\left(K - (K-1)(\frac{n-1}{n})^{0.5}\right) - (\frac{K-1}{K})(1 - (\frac{n-1}{n})^{0.5})} - \frac{2}{3K} \tag{26}$$

where n= 1.5 is for $\varepsilon_g \ge 0.476$ and n = $4\sqrt{3}$ for $\varepsilon_g \le 0.26$.

B is determined by the relation:

$$B = 1.25\left(\frac{1-\varepsilon_g}{\varepsilon_g}\right)^{10/9} \tag{27}$$

The dimensionless parameter $d_p h_p/k_g$ represents the heat transfer through the contact surface between particles, where d_p is the mean particle diameter in m, h_p denotes the heat transfer coefficient, representing the heat transfer rate through the contact surface between particles in W/(m^{2}K) (Qian et al., 2018).

For the ZS model, Γ is a combination parameter calculated as (Zehner and Schlünder, 1970):

$$\Gamma = \frac{2}{1-\frac{B}{K}}\left[\frac{K-1}{(1-\frac{B}{K})^2}\frac{B}{K}\ln\left(\frac{K}{B}\right) - \frac{B-1}{1-\frac{B}{K}} - \frac{1}{2}(B+1)\right] \tag{28}$$

For the ZBS model, ω is mainly affected by the packing arrangements and contact radius:

$$\omega = \frac{A_c/N_p}{\pi d_p^2/4} \tag{29}$$

where, the total contact area of all particles A_c in the bed domain divided by the number of particles N_p in the domain to obtain the average contact area of a single particle. Afterward, the division is performed by the cross-sectional area of the diameter of the equivalent volume sphere. In the case of assuming particles that are perfectly spherical and in direct contact, the contact area can be simplified to πd_p^2.

3. Results and discussion

The comparison between the simulations and experiments from Vargas et al. (Vargas and McCarthy, 2001) can be seen by the normalized temperature and normalized bed height shown in Fig. 6:

Both heights and temperature were normalized for every particle of the bed. Temperatures were averaged for intervals of 0.05. The results, consequently, report the average temperature on the bed height. The simulation errors originate from the variation of the simulation results attributed to the configuration of the particle bed. A good agreement was obtained by adjusting the simulation parameters based on the 155-minute experiment, resulting in an average R^2 value of 0.95. However, it should be noted that this value varied significantly depending on the arrangement of the particle bed being evaluated. The agreement was kept constant by the heat transfer coefficient being set as 350 W/m^{2}K and the thermal conduction resistivity factor as 1.5 (seen in Eq. (3)). Similarly, 1.5 was used for the effective resistivity factor ($f_{res,eff}$) on the particle-particle simulation model (seen in Eq. (4)) and the scaling parameter for mass-length-dependent heat transfer (S_l) was kept as 1.

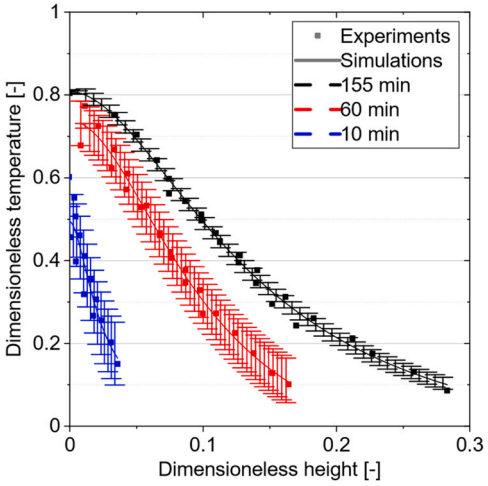

Fig. 6. Comparison between developed simulation and experiments from Vargas et al. (Vargas and McCarthy, 2001).

Comparing the temperature for the 60- and 10-min experiment led to an average agreement of an R^2 of 0.92 and 0.88, respectively. Shorter experiments (10 and 60 min) may introduce complexities as a result of transient behavior and dynamic effects, resulting in slightly lower R^2 values. The adjustments made based on the 155-minute experiment may not capture these transient behaviors perfectly for shorter durations. The R^2 with the 10- min experiment indicates a reasonable agreement, although it is lower than the previous cases. Additionally, other inaccuracies might be associated with the applied time factor to minimize the simulation time.

The simulations are significantly affected by the variation resulted from the packing arrangement. Efficiency of heat transfer within the particle bed can be enhanced by optimal packaging. In order to enhance the overall efficiency of heat transfer, it would be beneficial to create more effective channels for heat conduction within the bed. Alternatively, various arrangements can result in less effective routes for conducting heat, which provide an explanation for the fluctuations observed in the simulation results.

Moreover, the contact points or regions where particles come into contact with each other are altered by employing various particle arrangements. Modifying the contact surfaces can change the trajectories and speeds at which heat is exchanged between adjacent particles.

The influence on the compressive load on the thermal conductivity of the bed can be seen in Fig. 7 comparing the experiment and simulations:

The increased applied external load increases the effective conductivity, which can be explained by the increased contact pressure, improved particle contact, and decreased void space. As the load increases, conduction pathways are favored, resulting in a higher overall effective thermal conductivity. This trend can be seen in both experiments and simulations. The difference between experiments and simulations, encompassing all simulations, varied from 1.9% to 38.2%, with

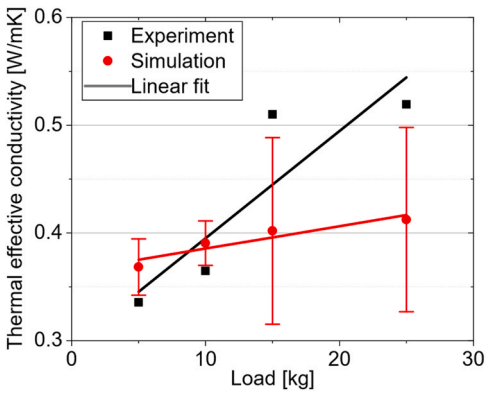

Fig. 7. Comparison between simulations and experiments from Vargas et al. (Vargas and McCarthy, 2001) for the thermal effective conductivity for different applied loads.

an average difference of 14.1%. The higher deviations occur with higher compressive loads. This deviation can be explained by several factors, including particle packing, particle deformation and fracture, and complex contact physics that are not fully described in the simulation scene. The creation of particle packing in a stochastic way contributes to a certain level of variance between experimental and simulated results, given the heat transfer model relies directly on the arrangement of particles, their interactions and structural uniformity within the packed bed. The significant deviations observed in the simulation values confirm the strong impact of particle packing within the bed on the heat transfer mechanism. By calculating the mean temperature at the same bed height, this variable is reduced, although it continues to exert a substantial influence.

Another notable observation pertains to the assumption made in the simulation regarding the presence of a monosized particle pack, which does not represent entirely the reality. Furthermore, all simulations with different applied loads were carried out based on the initial calibration performed for the 155-minute experiment, which included calibration of particle-particle model parameters such as thermal conduction resistivity factor, maximum and minimum overlap factor that could be influenced during compression. The good agreement between the simulations and experiments highlights the significance of heat conduction through stainless-steel spheres in the system. It further validates the proposed straightforward approach on the implemented models that incorporates a scaling parameter for mass-length-dependent heat transfer and effective thermal conduction resistivity factor. Which solution is more simplified in comparison to the solutions found in literature. The observed positive correlation and effective resolution can likely be attributed to the material composition of the sphere, namely the notable heat conductivity properties exhibited by stainless steel.

The models presented in Table 3 were utilized to model the effective thermal conductivity. The obtained values for the experiments of Vargas et al. (Vargas and McCarthy, 2001) can be seen in Table 4:

The lack of available data on changes in porosity and particle deformation is the main reason for the inability to monitor the fluctuations in effective thermal conductivity under different loads. However, it is noticeable that there was an observed rise in effective thermal conductivity from the modeled values to those obtained using experiments and simulation. It is anticipated that there will be variations in results as a result of the assumptions used in the modeling process, such as the assumption of perfectly spherical particles, the estimation of contact area, and the assumption of pack homogeneity. Nevertheless, the same order of magnitude between the values is observed and the values vary considerably according to the models.

Table 4
Effective thermal conductivity of the experiments from Vargas et al. (Vargas and McCarthy, 2001) modelled according to literature models.

Model	Effective thermal conductivity [W/mK]
Parallel layers	0.201
Series layers	0.094
Geometric mean	0.235
Kunii and Smith (KS)	0.210
Zehner and Schlünder (ZS)	0.249
Zehner-Bauer-Schlünder (ZBS)	0.251

When calculating the coefficient h_p for the Kunii and Smith model, the contact area and the morphology effect must be considered. Given the difficulty in determining both parameters experimentally, the model application for determining effective thermal conductivity is jeopardized. Qian et al. (Qian et al., 2018) came to the same conclusion, although previous authors widely used the model (Nield, 1991; Vargas and McCarthy, 2001).

The comparison between simulations and carried experiment with 165 μm glass particles from Mishra et al. (Mishra et al., 2019) can be seen in Fig. 8:

Higher distances from the wall result in greater error, which may be correlated with inappropriately adjusted parameters from the particle-particle model rather than the adjustment of particle-wall model parameters. Furthermore, it is evident that the simulations exhibit greater deviations as the distance from the wall increases, emphasizing the impact of packing on the heat transfer process. Nevertheless, a good agreement can be observed between simulation and experiments with a R^2 of 0.95. The time factor used to reduce simulation times had no effect on the simulation results, and compensation with the heat transfer particle wall could be performed. In order to ensure the simulation remains accurate when considering a time factor of $1 \bullet 10^3$, the model parameters were adjusted accordingly. The heat transfer coefficient for the particle-wall model was adjusted to $1 \bullet 10^6$ and the resistivity factor was set to 1. The particle-particle heat transfer model was modelled so the effective resistivity factor was 1, whereas the scaling parameter for mass-length-dependent heat transfer (S_l) was kept as $1 \bullet 10^6$. The same scale was kept of the convective heat transfer coefficient. The adjustments were made to ensure that the simulation results remained consistent with the original heat transfer behavior while maintaining physical accuracy with the applied time factor.

Fig. 9 compares the modelled heat transfer coefficient (h) from simulations and experiments for the different particle sizes and material:

In addition to the stainless steel spheres system provided by Vargas et al. (Vargas and McCarthy, 2001), the propose model for heat transfer also yielded good results when employing for all different systems with an average R^2 value of 0.93. Significant variations in the simulation

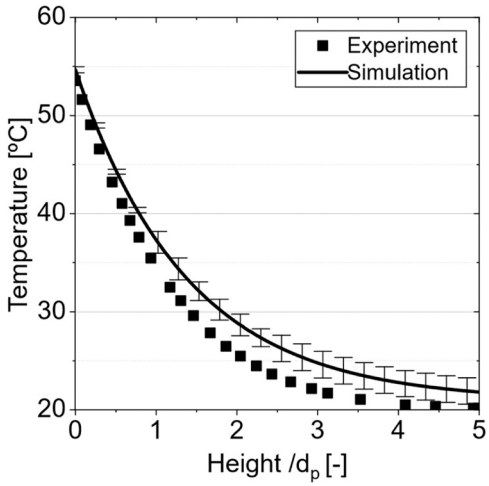

Fig. 8. Comparison between simulation and experiments of 165 μm glass particles Mishra et al. (Mishra et al., 2019).

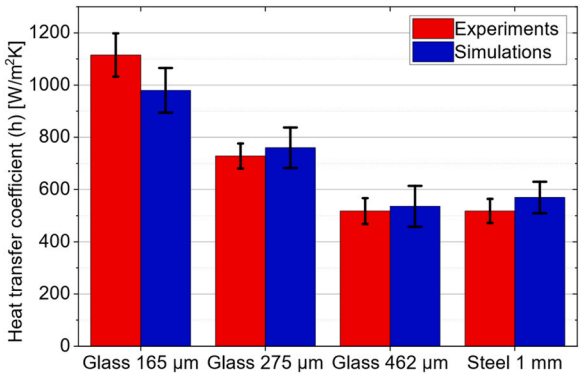

Fig. 9. Comparison between heat transfer coefficients obtained by simulations and experiments from Mishra et al. (Mishra et al., 2019).

results stem from the different particle packings, which directly impacts the heat transfer process. The variation is significantly larger in the system with a particle size of 165 µm, which presents the smallest size.

As particle size increased, the heat transfer coefficient decreased. This can be justified by the reduced surface area as large particles have smaller surface area-to volume ratio compared to smaller particles (Slavin et al., 2000a). Furthermore, larger particles frequently have thicker boundary layers of stagnant fluid that act as an insulator and reduce the rate of heat transfer (Tsory et al., 2013). This explanation also is supported by the determined modelled convective heat transfer coefficients. The increase in convective heat loss observed in the smallest particle sizes can be attributed to the improved contact between the particles and the fluid passing through the bed. As a result, there is an increased occurrence of interactions between the fluid and particles, which enhances the transfer of heat and ultimately leads to higher convective coefficients. Furthermore, smaller particles generally exhibit lower fluid flow resistance in comparison to larger particles. This leads to decreased pressure gradients and increased fluid velocity in close proximity to the particles, thereby augmenting convective heat transfer through enhanced fluid-particle interaction (Qu et al., 2022).

Another significant observation is that, for simplification, the Nusselt number was assumed to be constant throughout the entire simulations and, consequently, the convective heat transfer coefficient. However, as emphasized by Eq. (16), the Grashof number is directly proportional to the temperature difference between the particle bed and the fluid, meaning it does not remain constant throughout the simulation.

Similarly, the models presented in Table 3 were utilized to model the effective thermal conductivity. The heat transfer coefficient obtained from the models of the literature Eq. (14), can be compared to the simulations and experiments of the different systems of Mishra et al. (Mishra et al., 2019). The obtained values can be seen in Table 5:

A significant variation is evident in the heat transfer coefficient values derived from literature models compared to those obtained through DEM simulations and experiments. One of the significant reasons is the lack of consideration given to literature models that incorporate various factors influencing heat transfer in packed beds, including particle-particle interactions, non-uniform packing, and surface roughness. These factors have the potential to significantly deviate from both simulated and experimental results. In this context, the simulation exhibited a higher degree of resemblance to the experimental results when compared to the previously suggested models found in the existing literature.

Table 5
Effective thermal conductivity of the experiments from Mishra et al. (Mishra et al., 2019) for the glass particles of 165 µm, 275 µm and 462 µm and 1 mm steel particles modelled according to literature models.

Model	Heat transfer coefficient [W/m²K]			
	165 µm	275 µm	462 µm	1 mm
Parallel layers	103.34	102.51	111.54	609.77
Series layers	30.85	30.60	33.29	5.81
Geometric mean	88.05	87.34	95.03	420.48
Kunii and Smith (KS)	138.39	137.25	149.30	18.95
Zehner and Schlünder (ZS)	91.94	91.19	99.22	353.14
Zehner-Bauer-Schlünder (ZBS)	91.94	91.19	99.22	353.23

The proposed models highlighted the significance of inter-particle heat conduction as the main determinant of heat conduction in particle beds with stagnant fluid. Nevertheless, the impact of convective heat transfer is clearly apparent, particularly when examining particle systems of smaller sizes. The application of a resistance factor, along with the consideration of a scaling factor, demonstrates comparable applications for both systems including glass particles and stainless steel, thereby emphasizing a wide range of potential uses. This was further validated by the implementation of external forces on the experiments by Vargas et al. (Vargas and McCarthy, 2001), which result in increased contact pressure and enhanced particle interaction under greater loads, promoting the formation of efficient conduction pathways and substantially enhancing the overall heat conductivity.

Upon doing a comparative analysis of the two examined systems, it becomes apparent that the phenomenon of conduction between two particles is considered significant only when they are in close proximity to each other. As the thermal conductivity of the particles increased, the impact of indirect conduction diminished, while the importance of direct conduction via particle-particle interactions grew stronger. The study revealed that the effects of different conduction channels had a limited responsiveness to fluctuations in bed temperature. However, the importance of different conduction mechanisms in packed beds is greatly dependent on the layout of the packing structure. This is apparent through the varying simulation values that arise from different particle packings.

Despite it has been reported that conventional DEM models overpredict the contact radius and contact time (Peng et al., 2020), and the limitations of proposed correction factors such as the Zhou-Yu-Zulli method (Zhou et al., 2010) in compensating for the overestimated heat transfer caused by unrealistic particle material properties, the proposed simplified application has been successfully validated for stationary particle beds in this specific context. For more complex systems, with multi-body collisions and different collisional events (e.g. rolling and rest of particle clusters against the wall), further investigations are required.

The main drawback relies on the determinations of the required resistivity factor, scaling parameter for mass-length-dependent heat transfer and resistivity factor of the effective thermal conduction. These parameters depend on various factors within the system, including interparticle contacts, voids, packing conditions, particle shape as well as specific interactions between particles.

The results highlight the advantages on DEM simulations compared to continuous approach simulations despite their higher computational costs. While the continuum approach may provide accurate predictions for heat transfer within packed beds, the proposed model can capture granular behavior at a micro-scale level by modelling individual particle interactions, granular rearrangements, and complex contact physics, offering a more detailed and realistic representation of the system. This microscopic insight allows for a deeper understanding of particle-scale phenomena such as particle deformation, packing dynamics, and the influence of contact forces on heat transfer. It also provides valuable insights into localized phenomena and heterogeneities within the packed bed, which might not be adequately captured by the continuum approach. This detailed understanding from DEM simulations contributes to refining and improving macroscopic models, aiding in the development of more accurate continuum-based predictions for heat transfer in packed beds.

4. Conclusion

The utilization of granular media spans across multiple industries. Due to their distinct behavior compared to single-phase systems, the examination, development, and optimization of industrial processes, as well as the comprehension of natural phenomena, heavily depend on the physicochemical and transport properties of these materials. On this work, heat transfer models for particle-wall and particle-particle for particle beds for different material systems were implemented on MUSEN open source framework.

The implemented particle-particle and particle-wall models were validated on experimental data by Vargas et al. (Vargas and McCarthy, 2001) and Mishra et al. (Mishra et al., 2019). Simulation scenes were created to replicate the experimental conditions. Both experimental setups were simulated with good agreement. The simulations had a high agreement for the experimental proposed by Vargas et al. (Vargas and McCarthy, 2001), with R^2 of 0.95 for the 155- minute experiment, R^2 of 0.92 and for the 60- minute experiment, and R^2 of 0.88 for the 10-minute experiment. The effective thermal conductivity simulated and experimental for various compressive loads also showed good agreement, with an average deviation of 14.1%.

Similarly, when comparing simulations and experiments proposed by Mishra et al. (Mishra et al., 2019), a good agreement was obtained. The simulations for the system of glass particles with 165 μm presented an R^2 of 0.9. When comparing the heat transfer coefficients of the other systems and simulations, the average error was 7.5%.

The relevance of inter-particle heat conduction as the primary factor influencing heat conduction in particle beds with stagnant fluid was emphasized by the proposed models. However, it is evident the influence of convective heat transfer, especially when considering smaller particle systems. As a result, the manner in which a bed is packed has a direct impact on various conduction mechanisms and this variability between simulations and experiments may lead to the difference observed between them.

In addition to the good simulation agreement, the simulation times on the MUSEN framework could be reduced being similar to simulations in a continuum approach. As a result, the proposed models on MUSEN have a high potential for investigating heat transfer phenomena in particle beds. The combination of speed and accuracy allows for more in-depth analyses and a broader range of applications, making it an invaluable tool for heat transfer in different systems.

Declaration of Competing Interest

The authors declare that they have no known competing financial interests or personal relationships that could have appeared to influence the work reported in this paper.

Acknowledgements

We gratefully acknowledge the financial support of DFG Graduate School GRK 2462 Processes in natural and technical particle fluid systems (PintPFS) (Project No. 390794421). We thank Mr. Vasyl Skorych for the assistance and model implementation.

References

Alves, C.L., Skorych, V., Noni, A., de, Hotza, D., González, S.G., Heinrich, S., 2023. Microscale DEM simulation of spray-dried porcelain granules under uniaxial compaction. Powder Technol. 428, 118863 https://doi.org/10.1016/j.powtec.2023.118863.

Atrian, A., Lund, J., Radtke, L., Skorych, V., Dosta, M., Düster, A., 2021. A partitioned scheme for coupling of FEM and DEM simulations of granular materials. Proc. Appl. Math. Mech. 21, e202100134 https://doi.org/10.1002/pamm.202100134.

Batchelor, G.K., O'Brien, R.W., 1977. Thermal or electrical conduction through a granular material. Proc. R. Soc. Lond. Ser. A 355, 313–333. https://doi.org/10.1098/rspa.1977.0100.

Bauer, R., 1978. Schlunder, effective radial thermal conductivity of packings in gas flow. Part II thermal conductivity of the packing fraction without gas flow. Int. Chem. Eng. 18, 189–204.

Besler, R., Rossetti da Silva, M., do Rosario, J.J., Dosta, M., Heinrich, S., Janssen, R., 2015. Sintering simulation of periodic macro porous alumina. J. Am. Ceram. Soc. 98, 3496–3502. https://doi.org/10.1111/jace.13684.

Borkink, J.G.H., Westerterp, K.R., 1992. Influence of tube and particle diameter on heat transport in packed beds. AIChE J. 38, 703–715.

Cheng, G., Gan, J., Xu, D., Yu, A., 2020. Evaluation of effective thermal conductivity in random packed bed: Heat transfer through fluid voids and effect of packing structure. Powder Technol. 361, 326–336. https://doi.org/10.1016/j.powtec.2019.07.106.

Dai, W., 2019. Thermal conduction in granular media: from interface, topology to effective property.

Deissler, R.G., Boegli, J.S., 1958. An investigation of effective thermal conductivities of powders in various gases. J. Fluids Eng. 80, 1417–1423. https://doi.org/10.1115/1.4012740.

Dosta, M., Skorych, V., 2020. MUSEN: an open-source framework for GPU-accelerated DEM simulations. SoftwareX 12, 100618. https://doi.org/10.1016/j.softx.2020.100618.

Dosta, M., Weber, M., Schmidt, V., Antonyuk, S., 2019. DEM analysis of breakage behavior of bicomponent agglomerates. Part. Contact. Micro Mech. Micro Process Dyn. Part. Collect. 165–183.

Dosta, M., Furlan, K.P., Skorych, V., Heinrich, S., Janssen, R., 2020. Influence of pores arrangement on stability of photonic structures during sintering. J. Eur. Ceram. Soc. 40, 4562–4571. https://doi.org/10.1016/j.jeurceramsoc.2020.04.019.

Druma, A.M., Alam, M.K., Druma, C., 2004. Analysis of thermal conduction in carbon foams. Int. J. Therm. Sci. 43, 689–695.

Fischer, J., Rodrigues, S.J., Kriegeskorte, M., Hilse, N., Illana, E., Scherer, V., Tsotsas, E., 2023. Particle-particle contact heat transfer models in thermal DEM: a model comparison and experimental validation. Powder Technol. 429 https://doi.org/10.1016/j.powtec.2023.118909.

Froment, G.F., Bischoff, K.B., Wilde, J. de, 1990. Chemical reactor analysis and design. Wiley New York.

Graczykowski, B., El Sachat, A., Reparaz, J.S., Sledzinska, M., Wagner, M.R., Chavez-Angel, E., Wu, Y., Volz, S., Alzina, F., Sotomayor Torres, C.M., 2017. Thermal conductivity and air-mediated losses in periodic porous silicon membranes at high temperatures. Nat. Commun. 8, 415. https://doi.org/10.1038/s41467-017-00115-4.

Jarolin, K., Dymala, T., Heinrich, S., Dosta, M., 2022. Modeling the devolatilization and fragmentation of biomass pellets with the bonded particle method for fluidized bed applications. Comp. Part. Mech. 9, 1319–1335. https://doi.org/10.1007/s40571-022-00467-9.

Jayachandran, S., Reddy, K.S., 2019. Estimation of effective thermal conductivity of packed beds incorporating effects of primary and secondary parameters. Therm. Sci. Eng. Prog. 11, 392–408. https://doi.org/10.1016/j.tsep.2018.12.011.

Kaviany, M., 2012. Principles of Heat Transfer in Porous Media. Springer Science & Business Media.

Kunii, D., Smith, J.M., 1960. Heat transfer characteristics of porous rocks. AIChE J. 6, 71–78. https://doi.org/10.1002/aic.690060115.

Mishra, I., Lattanzi, A.M., LaMarche, C.Q., Morris, A.B., Hrenya, C.M., 2019. Experimental validation of indirect conduction theory and effect of particle roughness on wall-to-particle heat transfer. AIChE J. 65, e16703.

Nield, D.A., 1991. Estimation of the stagnant thermal conductivity of saturated porous media. Int. J. Heat. Mass Transf. 34, 1575–1576. https://doi.org/10.1016/0017-9310(91)90300-4.

Peng, Z., Doroodchi, E., Moghtaderi, B., 2020. Heat transfer modelling in discrete element method (DEM)-based simulations of thermal processes: theory and model development. Prog. Energy Combust. Sci. 79, 100847 https://doi.org/10.1016/j.pecs.2020.100847.

Presley, M.A., Christensen, P.R., 1997. Thermal conductivity measurements of particulate materials 1. A review. J. Geophys. Res.: Planets 102, 6535–6549.

Qian, Y., Han, Z., Zhan, J.-H., Liu, X., Xu, G., 2018. Comparative evaluation of heat conduction and radiation models for CFD simulation of heat transfer in packed beds. Int. J. Heat. Mass Transf. 127, 573–584. https://doi.org/10.1016/j.ijheatmasstransfer.2018.06.127.

Quentrec, B., Brot, C., 1973. New method for searching for neighbors in molecular dynamics computations. J. Comput. Phys. 13, 430–432. https://doi.org/10.1016/0021-9991(73)90046-6.

Rodrigues, S.J., Vorhauer-Huget, N., Tsotsas, E., 2022. Effective thermal conductivity of packed beds made of cubical particles. SSRN J. https://doi.org/10.2139/ssrn.4034396.

Rong, D., Horio, M., 1999. DEM simulation of char combustion in a fluidized bed. Second International Conference on CFD in the Minerals and Process Industries. CSIRO, Melbourne, Australia, pp. 65–70.

Sarikaya, O., Islamoglu, Y., Celik, E., 2005. Finite element modeling of the effect of the ceramic coatings on heat transfer characteristics in thermal barrier applications. Mater. Des. 26, 357–362.

Slavin, A.J., Londry, F.A., Harrison, J., 2000a. A new model for the effective thermal conductivity of packed beds of solid spheroids: alumina in helium between 100 and 500C. Int. J. Heat. Mass Transf. 43, 2059–2073.

Slavin, A.J., Londry, F.A., Harrison, J., 2000b. A new model for the effective thermal conductivity of packed beds of solid spheroids: alumina in helium between 100 and 500C. Int. J. Heat. Mass Transf. 43, 2059–2073.

Teixeira, M.H.P., Skorych, V., Janssen, R., González, S.Y.G., Noni Jr, A., de, Rodrigues, Neto, J.B., Hotza, D., Dosta, M., 2021. High heating rate sintering and

microstructural evolution assessment using the discrete element method. Open Ceram. 8, 100182 https://doi.org/10.1016/j.oceram.2021.100182.
Tsory, T., Ben-Jacob, N., Brosh, T., Levy, A., 2013. Thermal DEM–CFD modeling and simulation of heat transfer through packed bed. Powder Technol. 244, 52–60. https://doi.org/10.1016/j.powtec.2013.04.013.
Tsotsas, E., 2019. Particle-particle heat transfer in thermal DEM: three competing models and a new equation. Int. J. Heat. Mass Transf. 132, 939–943. https://doi.org/10.1016/j.ijheatmasstransfer.2018.12.090.
Tsotsas, E., Martin, H., 1987. Thermal conductivity of packed beds: a review. Chem. Eng. Process. 22, 19–37. https://doi.org/10.1016/0255-2701(87)80025-9.
Vargas, W.L., McCarthy, J.J., 2001. Heat conduction in granular materials. AIChE J. 47, 1052–1059. https://doi.org/10.1002/aic.690470511.
Verlet, L., 1967. Computer "experiments" on classical fluids. I. Thermodynamical properties of Lennard-Jones molecules. Phys. Rev. 159, 98–103. https://doi.org/10.1103/PhysRev.159.98.
Wu, H., Gui, N., Yang, X., Tu, J., Jiang, S., 2021. Parameter analysis and wall effect of radiative heat transfer for CFD-DEM simulation in nuclear packed pebble bed. Exp. Comput. Multiph. Flow. 3, 250–257. https://doi.org/10.1007/s42757-020-0058-2.
Yagi, S., Kunii, D., 1957. Studies on effective thermal conductivities in packed beds. AIChE J. 3, 373–381. https://doi.org/10.1002/aic.690030317.
Zehner, P., Schlünder, E.U., 1970. Wärmeleitfähigkeit von Schüttungen bei mäßigen Temperaturen. Chem. Ing. Tech. 42, 933–941. https://doi.org/10.1002/cite.330421408.
Zhou, Z.Y., Yu, A.B., Zulli, P., 2010. A new computational method for studying heat transfer in fluid bed reactors. Powder Technol. 197, 102–110. https://doi.org/10.1016/j.powtec.2009.09.002.